Journal Pre-proof

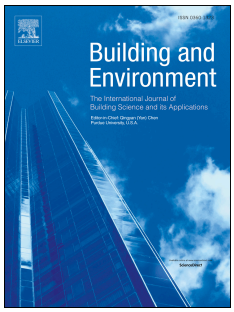

Mitigating intensity of urban heat island by better understanding on urban morphology and anthropogenic heat dispersion

Chao Yuan, Ayu Sukma Adelia, Shuojun Mei, Wenhui He, Xian-Xiang Li, Leslie Norford

PII: S0360-1323(20)30235-3

DOI: https://doi.org/10.1016/j.buildenv.2020.106876

Reference: BAE 106876

To appear in: *Building and Environment*

Received Date: 18 February 2020

Revised Date: 31 March 2020

Accepted Date: 2 April 2020

Please cite this article as: Yuan C, Adelia AS, Mei S, He W, Li X-X, Norford L, Mitigating intensity of urban heat island by better understanding on urban morphology and anthropogenic heat dispersion, *Building and Environment* (2020), doi: https://doi.org/10.1016/j.buildenv.2020.106876.

Mitigating Intensity of Urban Heat Island by Better Understanding on Urban Morphology and Anthropogenic Heat Dispersion

Chao Yuan[1]*, Ayu Sukma Adelia[1], Shuojun Mei[1], Wenhui He[1], Xian-Xiang Li[2,4,5],Leslie Norford[3]

1. Department of Architecture, National University of Singapore, Singapore
2. School of Atmospheric Sciences, Sun Yat-sen University, Guangdong, China
3. Department of Architecture, Massachusetts Institute of Technology, Massachusetts, USA
4. Southern Marine Science and Engineering Guangdong Laboratory (Zhuhai), China
5. Guangdong Province Key Laboratory for Climate Change and Natural Disaster Studies, Sun Yat-sen University, China

Abstract:

Anthropogenic heat is one of the key factors that causes intensive Urban Heat Island (UHI) due to its direct impact on ambient temperature in urban areas. Stagnated airflow due to closely packed tall buildings causes weak dilution and removal of anthropogenic heat. Consequently, research is critically needed to investigate the effect of urban morphology on anthropogenic heat dispersion and provide effective planning strategies to reduce UHI intensity, especially at the extreme scenarios, such as with very low wind speed and high heat emission. This study provides scientific understanding and develops a Geographic Information System (GIS)-based modelling tool to support decision-making in urban planning practice. We start from a computational parametric study at the neighbourhood scale to investigate the impact of urban morphology on heat dispersion. Site coverage ratio and frontal area density are two urban morphological parameters. Ten parametric cases with two heat emission scenarios are designed to study representative urban areas. Furthermore, based on the energy conservation within urban canopy layers, we develop a semi-empirical model to estimate spatially-averaged in-canopy air temperature increment, in which the exchange velocity between street canyons and overlying atmosphere is estimated by the Bentham and Britter model. The performance of new model is validated by cross-comparing with Computational Fluid Dynamics (CFD) results from the parametric study. By applying this new model, the impact of anthropogenic heat on air temperature is mapped in residential areas of Singapore for both long-term annually averaged and short-term extreme low wind speed to improve urban climate sustainability and resilience.

Key words:

Anthropogenic heat dispersion, Semi-empirical model, CFD simulation, Urban planning, GIS mapping

Nomenclature:

A_{Ap}	apartment area (m^2)
A_i	surface area of certain element type (m^2)
A_p	building footprint (m^2)
A_f	frontal area approached by the incoming wind (m^2)
A_{floor}	floor/building footprint area (m^2).
A_T	site area (m^2)
$\mathrm{A_{Ap}}$	apartment area (m^2)
$A_{opening}$	opening area of urban canopy (m^2)
c_p	specific heat capacity of air ($J\ K^{-1}kg^{-1}$)
COP	coefficient of AC performance (-)
D_c	model constant related to air heat capacity ($J\ K^{-1}m^{-3}$)
E_c	AC operation energy (kW)
Fr	Froude number (-)
g	gravitational acceleration (m/s^2)
Gr	Grashof number (-)
H	height of street canyon (m)
H/W	canyon aspect ratio (-)
κ	turbulence kinetic energy (m^2/s^2)
L	building length (m);
n_{HDB}	number of HDB building blocks
$\frac{Q_{A\_site}}{Q_{A\_Singapore}}$	heat emission intensity normalized by site area (kW/m^2)
$\overline{Q_A}$	averaged anthropogenic heat generated from per apartment at Singapore (kW)
Q_A	anthropogenic heat per apartment (kW)
$\overline{Q_s}$	anthropogenic heat intensity per m^2 (kW/m^2)
$\overline{Q_c}$	sensible heat (kW)
Q	average cooling load (kW)
Q_{roof}	heat emission rate of urban canopy unit (kW)
Re	heat flux at roof level (kW)
Ri	Reynolds number (-)
T_0	Richardson number (-)
T_0	in-canopy air temperature (C^o)
T_w	ambient air temperature (C^o)
ΔT_c	temperature of the heated surfaces (C^o)
ΔT_p	In canopy air temperature increment (C^o)
$T_{emission}$	Air temperature increment at the pedestrian level, 2m above the ground (C^o)
$T_{increment}$	emission air temperature (C^o)
u_*	emission temperature increment of the releasing hot air from the condenser (C^o)
u^*_{ABL}	friction velocity at built-up area (m/s)
U_c	atmospheric boundary layer friction velocity (m/s)
U_E	in-canopy velocity of urban canopy layer (m/s)
U_h	exchange velocity of urban canopy layer (m/s)
U_{met}	wind speed at the height, (m/s)
U_{ref}	wind speed at reference height d_met = 300m (m/s)
W	reference wind velocity (m/s)
z	width of street canyon (m)
z_0	height above the ground (m)
z_d	Roughness length (m)
α	Displacement height (m)
β	surface roughness coefficient (-)
ε	volumetric expansion coefficient of air (K^{-1})
λ_i	turbulence dissipation rate (m^2/s^3)
λ_p	urban planning indices (-)
λ_f	site coverage ratio (-)
ρ	frontal area density (-)
ν	air density (Kg/m^3)
	kinematic viscosity of the air m^2/s

1. Introduction

With rapid urbanization, the urban heat island (UHI) effect has caused serious environmental challenges to both urban climate sustainability and resilience. Anthropogenic heat emission is one of the key factors that causes intensive UHI due to its direct impact on ambient temperature in urban areas (Chow and Roth, 2006; Oke, 1988). A Weather Research and Forecasting (WRF) modelling study conducted by Singapore-MIT Alliance for Research and Technology (SMART) indicates that the impact of anthropogenic heat on ambient air temperature is significant in the Central Business District, Singapore (Li and Norford, 2016). Chow and Roth (2006) studied the temporal UHI of Singapore and concluded that UHI in Singapore is influenced by a combination of site-specific factors, such as low wind speed and intense anthropogenic heat emission.

Many studies indicated that urban morphology has a significant impact on urban outdoor environment through modification on momentum, mass, and heat transfer around urban structures (Chen et al., 2017; Givoni, 1998; Hang et al., 2017; Oke, 1988; Tominaga and Stathopoulos, 2016). Weak anthropogenic heat removal and dilution within the street canyon is caused by stagnated airflow around closely packed and tall buildings. Therefore, effective strategies for anthropogenic heat removal and dilution are crucial to reduce the magnitude of the UHI. There are a lot of existing studies on air flow itself at high density urban areas. However, it could be difficult, and even wrong, if we directly apply the knowledge on air flow to estimate the anthropogenic heat dispersion. Hence, research is critically needed to investigate the effects of urban morphology on anthropogenic heat dispersion at urban areas.

Computational Fluid Dynamics (CFD) simulation can provide accurate and high resolution modelling results of heat transfer and dispersion in the street canyon, and thus evaluate the effect of anthropogenic heat on air temperature. The numerical study conducted by (Sini et al., 1996) showed that differential heating can shift the in-street flow structure from one-vortex flow to several counter-rotating vortices, and Mei et al. (2016) indicates that buoyancy force induced by heated urban surfaces significantly alters temperature distribution inside street canyon. Kim and Baik (2001) carried out extensive CFD simulations with various street canyon aspect ratios and street-level heating to characterize the flow regime. Oliveira Panão et al. (2009) applied a two-dimensional simulation to study the influence of a windward-heated wall on the airflow circulation in a street canyon with building height-to-street width ratio (H/W aspect ratio) from 0.7 to 1.5. The modelling results identified three airflow regimes. Regime (I) includes a single circulatory flow within street canyons. Regime (I) occurs for high wind intensities when the circulatory flow dominates

over the thermal flow. By decreasing the Froude number ($Fr = \frac{Re^2}{Gr}$, where Gr is the Grashof number and Re is the Reynolds number), the flow within street canyons shifts to regime (II), with two counter-rotating vortices co-existing inside the canyon. When further decreasing Fr number, the lower vortex dominates the air circulation inside street canyons, and it is defined as regime (III). Airflow regime III can efficiently remove the warm air inside the cavity due to a strong upward air current close to the surface opposite to the main flow direction. Rather than the above mentioned simulation work, Adelia et al. (2019) extended the anthropogenic heat study to the implementation of architectural design, by conducting a computational parametric study. Effects of building typologies on anthropogenic heat dispersion were investigated, and the understandings from this parametric study directly benefit the architectural design practice.

Apart from CFD simulation, wind tunnel and water channel experiments are also important approaches to model the flow and heat dispersion at urban areas. Ruck (1993) measured the flow field around isolated buildings with heated surfaces with a 2D Laser Doppler Anemometer (LDA), and experimental results showed a significant change in the recirculation zone when the heat release increased above $Gr/Re^2 = 0.2$. Uehara et al. (2000) conducted a wind tunnel experiment, and investigated the effects of bottom heating and cooling on flow in urban street canyons. Allegrini et al. (2013) used Particle Image Velocimetry (PIV) to measure street canyon flow with heated surfaces in a wind tunnel. They reproduced a secondary counter-rotating vortex under a heated windward wall condition, as Sini et al. (1996) found in CFD simulation. The wind tunnel experiment conducted by Cui et al. (2016) covered a range of Richardson numbers ($Ri = Gr/Re^2$) between 0 to 4.77, and investigated thermal effects on both airflow and pollutant dispersion. The above wind tunnel experiments are significant because they provided not only the experimental results to validate numerical simulations, but also new understandings on effects of buoyance force on air flow.

2. Research Objectives

This study aims to provide scientific understanding of anthropogenic heat dispersion at the urban scale and develop a practical GIS-based modelling tool to support decision-making in urban planning practice in tropical cities. This study is motivated by the needs of urban planning and design practice to make high density cities sustainable and resilient. The literature review indicates that both numerical and experimental approaches have been conducted to model and investigate heat dispersion. But both of them are not suitable for urban planning and design practice as they are computationally expensive and require intensive technical support, especially for modelling at the urban scale.

Therefore, we develop a semi-empirical model to address the existing gap between urban climatologists and urban planners. Grimmond and Oke (1999) conducted a comprehensive review of the relationship between morphological indices with urban aerodynamic properties, such as roughness length (z_0) and displacement height (z_d). Linear relationships between urban morphology with spatially averaged wind speed at the pedestrian level were also found by (Ng et al., 2011; Yim et al., 2009; Yoshie et al., 2008; Yuan et al., 2014; Yuan et al., 2016). Several semi-empirical models were also developed. Adolphe (2001) provided a practical GIS based tool to evaluate the urban climate performance. Based on the balance between drag force and momentum within urban canopy layer, Bentham and Britter (2003) developed a single layer model to predict the in-canopy velocity (U_c) and exchange velocity (U_E). The temporally and spatially averaged pollutant concentration within the street canyon could also be calculated by semi-empirical models. Soulhac et al. (2013) provided a realistic street network model to predict the pollutant concentration in the complex street networks. Yuan et al. (2019) developed a GIS-based multilayer urban canopy model to estimate the air pollutant concentration in high-density urban areas. This GIS based tool is much cheaper than both CFD simulation and wind tunnel experiment, and can be easily used as an urban planning tool.

First, In this study, we start from the computational parametric study, which is based on urban morphology parameterization and conducted by numerical CFD simulation (Section 3). Ten parametric cases within two heat emission scenarios are designed to represent real scenarios in high-density cities. Second, based on the understandings from the parametric study, a GIS-based semi-empirical model is developed as a practical planning tool to estimate the impact of anthropogenic heat dispersion on ambient air temperature (Section 4). A case study of Singapore is conducted at Section 5 as the implementation to clarify how to apply the new semi-empirical model in real urban areas and evaluate the impact of anthropogenic heat on air temperature at annually-average and extreme weather conditions.

It should be noted that urban anthropogenic heat emission sources can be classified as the sources of commercial, residential, and industrial buildings, transportation, and human body metabolism (Oke et al., 2017), and we only focus on residential areas, where people are living, in this study. This is because the increment of outdoor ambient air temperature at residential areas could affect indoor thermal comfort more significantly than at commercial areas, especially at night, when the residents could expect to enjoy the natural ventilation.

3. Computational Parametric Study

3.1 Urban morphology parameterization

This computational parametric study was conducted at the neighbourhood scale, similar with our previous studies (Adelia et al., 2019; Wai et al., 2020; Yuan and Ng, 2012; Yuan et al., 2014). Ten parametric cases with various urban morphologies were designed based on permutations of urban planning indices, i.e. site coverage ratio (λ_p), and frontal area density (λ_f). These two parameters are the ratio between element type (A_i), e.g. building footprint (A_p) and frontal area approached by the incoming wind (A_f), within the total site area (A_T). The parameters can be expressed as (Oke et al., 2017):

$$\lambda_i = \frac{A_i}{A_T} \quad (1)$$

Based on the above literature review on semi-empirical modelling in Section 2, λ_p and λ_f are considered to be critical parameters for mass and momentum transfer within urban boundary layer, and thus we applied these two morphological indices in this parametric study. With 48 building blocks in a 345,600 m^2 site, we kept land use density (i.e. plot ratio) constant and changed values of λ_p and λ_f by modifying building width and height, as shown in Table 1. Given the constant plot ratio, the value of λ_f increases as λ_p decreases. The average plot ratio for a high-density residential town (e.g. Housing & Development Board (HDB) housing) in Singapore varies from 2.8 - 4.2 (Tuan Seik, 2001). Considering the growing population trend, a plot ratio 6.0 was chosen for the future scenario in this study. The length of buildings is a constant 100 m, which is the average length of HDB blocks in Singapore (Adelia et al., 2019). Figure 1 shows 3D parametric models in Cases 1-10.

Table 1. Urban morphological parameters at 10 cases with the same plot ratio, 6.0.

Cases	A_T	n_{HDB}	L	W	H	A_{floor}	λ_p	λ_f
01	345600	48	100	48	30	4800	0.67	0.42
02				44	32	4400	0.61	0.44
03				40	36	4000	0.56	0.50
04				36	40	3600	0.50	0.56
05				32	45	3200	0.44	0.63
06				28	50	2800	0.39	0.69
07				24	60	2400	0.33	0.83
08				20	72	2000	0.28	1.00
09				16	90	1600	0.22	1.25
10				12	120	1200	0.17	1.67

Note: A_T: Site area (m^2); n_{HDB}: Number of HDB building blocks; L: Building length (m); W: Building width (m); H: Building height (m); A_{floor}: floor/footprint area (m^2).

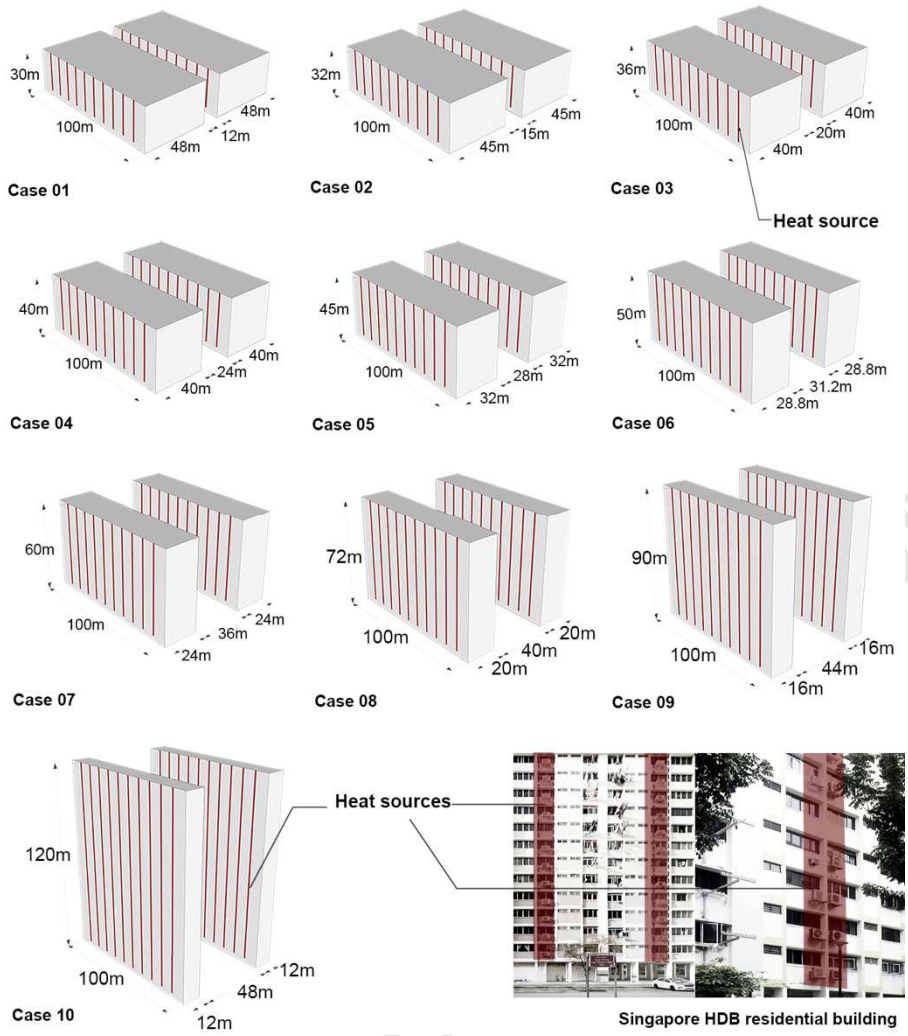

Figure 1 Ten parametric cases with various λ_p and λ_f. Heat emission sources are highlighted as red belts on buildings. The real Singapore HDB residential buildings and the heat emission locations are also included.

3.2 Estimation of anthropogenic heat emission

Apartment-based anthropogenic heat emission in typical HDB residential areas in Singapore was estimated based on the air-conditioner (AC) operation and heat conservation (Adelia et al., 2019). This study focuses on the nighttime scenario with anthropogenic heat emission from an HDB neighborhood, and assumes each apartment only uses one AC. We set up the anthropogenic heat emission at each building and apartment (Figure 1) using anthropogenic heat emission intensity $\mathrm{Q_A}$, the heat emission ($\overline{Q_{A\_Singapore}}$) normalized by average apartment area ($\mathrm{A_{Ap}}$). We did not directly apply $\overline{Q_{A\_Singapore}}$ to all the apartments in the parametric study, because the size of apartments ($\overline{Q_A}$) could be significantly different, and thus the emissions are also different. On the other hand, by using heat emission intensity $\mathrm{Q_A}$, we can keep the total anthropogenic heat emission the same in the 10 cases

for the cross-comparison. Average anthropogenic heat emitted per apartment in Singapore ($\overline{Q_{A\_Singapore}}$) can be calculated as (Kikegawa et al., 2003):

$$\overline{Q_{A\_Singapore}} = \overline{Q_c} + E_c \text{ , where } E_c = \overline{Q_c}/COP \quad (2)$$

where $\overline{Q_c}$ is the average cooling load, 2.5 kW, which is adopted from Energy Efficient Singapore (*http: //www.e2singapore.gov.sg*), and E_C is the AC operation energy, the quotient of $\overline{Q_c}$ and Coefficient of AC performance (COP), 3.34 (National Environemnt Agency (NEA), 2014). Thus the average anthropogenic heat emitted from each HDB apartment in Singapore ($\overline{Q_{A\_Singapore}}$) is 3.25 kW (Adelia et al., 2019). Therefore, given the average apartment unit area 200 m^2 in the parametric study, the heat emission intensity Q_A is 16.25 W/m^2.

As shown in Table 2, two arrangements were designed to make the parametric study representative to the real situation. In scenario I (Table 2a), the arrangement and number of apartment units are constant in all cases, i.e. single-loaded corridor with 10 apartment units per floor. This arrangement causes significantly different apartment unit areas, and thus different anthropogenic heat emission ($\overline{Q_A}$) per apartment, as shown in Table 2a. Because the condenser is air-cooled, $\overline{Q_A}$ is equal to sensible heat ($\overline{Q_s}$). Therefore, the temperature increment ($T_{increment}$) of the released hot air from the condenser in the 10 cases can be calculated as:

$$T_{increment} = \frac{\overline{Q_s}}{m \cdot c_p}, \text{where } \overline{Q_s} = \overline{Q_A}, \text{and } \overline{Q_A} = Q_A \cdot A_{AP} \quad (3)$$

where m is the air flow rate, 0.245 kg/s, c_p is the specific heat of air, 1.005 kJ/kg·K, A_{AP} is the apartment area m^2, and Q_A is the heat emission intensity, 16.25 W/m^2. Both $T_{increment}$ and $T_{emission}$, which is the sum of $T_{increment}$ and T_o(background air temperature), are presented in Table 2a.

Table 2a Heat emission scenario I with various A_{AP}, $\overline{Q_A}$ ($\overline{Q_s}$), $T_{increment}$, and $T_{emission}$

Cases (II)	A_{floor}	n_{AP}	A_{AP}	Heat source locations	$\overline{Q_A}$ ($\overline{Q_s}$)	T_0	$T_{increment}$	$T_{emission}$
1	4800	10	480	1 side	7.80	27	31.7	58.7
2	4400		440		7.15		29.0	56.0
3	4000		400		6.50		26.4	53.4
4	3600		360		5.85		23.8	50.8
5	3200		320		5.20		21.1	48.1
6	2880		288		4.68		19.0	46.0
7	2400		240		3.90		15.8	42.8
8	2000		200		3.25		13.2	40.2
9	1600		160		2.60		10.6	37.6
10	1200		120		1.95		7.9	34.0

Note: A_{floor}: floor area (m^2); n_{AP}: number of apartment; A_{AP}: apartment area; $\overline{Q_A}$: Anthropogenic heat emission per apartment (kW); $\overline{Q_s}$: Sensibile heat (kW); T_0: Background air temperature (C^o); $T_{increment}$: Temperature increment due to anthropogenic heat; $T_{emission}$: Emission air temperature (C^o).

In scenario II, we designed the apartment unit with the same A_{AP} by modifying the arrangement and number of units per floor with either single-loaded or double-loaded corridor. Therefore, all apartment areas (A_{AP}) are the same, 200 m^2, and the anthropogenic heat emission from each apartment ($\overline{Q_A}$) is constant. The constant values of $T_{increment}$ and $T_{emission}$ for the 10 cases in Scenario II are listed in Table 2b.

Table 2b Heat emission scenario II with constant A_{AP}, $\overline{Q_A}$ ($\overline{Q_S}$), $T_{increment}$, and $T_{emission}$

Cases (I)	A_{floor}	n_{AP}	A_{AP}	Heat source locations	$\overline{Q_A}$ ($\overline{Q_s}$)	T_0	$T_{increment}$	$T_{emission}$
1	4800	24	200	2 sides	3.25	27	13.2	40.2
2	4400	22						
3	4000	20						
4	3600	18						
5	3200	16						
6	2800	14						
7	2400	12		1 side				
8	2000	10						
9	1600	8						
10	1200	6						

Based on the above estimation, values of $T_{emission}$ for 10 cases were calculated in two scenarios. The $T_{emission}$ were used as the input boundary condition in the CFD simulation (Section 3.3). It should be noted that the analysis in this section also indicates that the building design, i.e. different building typology, affects not only the outdoor heat dispersion, but also intensity and distribution of anthropogenic heat emission.

3.3 Anthropogenic heat dispersion modelling

Anthropogenic heat dispersion for 10 parametric cases were modelled using CFD simulation by ANSYS Fluent. Each case consists of six columns and eight rows of 48 simplified HDB buildings, as shown in Figure 2. Heat emission was set up based on the estimation in Section 3.2, which is emission air temperatures ($T_{emission}$) listed in Table 2. The number and locations of heat emission sources are arranged based on the apartment layouts in the cases, as shown in Figure 1. The CFD simulation settings follow the Architectural Institute of Japan (AIJ) guidelines (Tominaga et al., 2008).

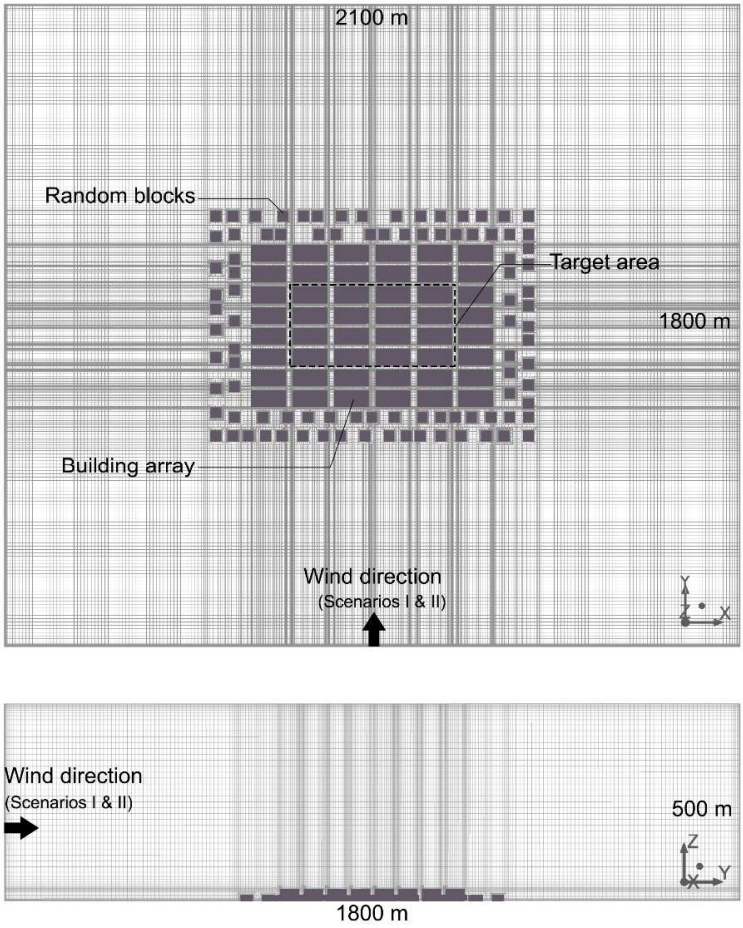

Figure 2. Modelling configurations for CFD simulation.

As shown in Figure 2, the computational domain size is 2100 (W) x 1800 (L) x 500 m (H). The distances between the inlet outlet and sides boundary to the edge of the building are set as 600 m, which is long enough for wake vortices development. The grid numbers are from 12 to 15 million hexahedral cells with maximum grid size ratio 1.2. The mesh close to building surfaces is refined with a minimum size of 0.23m. Clusters of buildings were added randomly around the study area to represent the surrounding urban context. Two approaching wind directions were considered, i.e. normal and parallel to the street canyon. A power law equation was applied for the incoming wind speed profile, i.e. time-averaged horizontal velocity, as:

$$\mathrm{U}_h = U_{met}(\frac{h}{\mathrm{d}_{met}})^{\alpha} \quad (5)$$

where U_h is the wind speed at the height (h), $U_{met}$is the reference wind speed, 7.4 m/s, at reference height d_met, 300m, and α is the surface roughness,0.3 (Adelia et al., 2019). The turbulence originates only from friction and shear as (Richards and Hoxey, 1993):

$$k(z) = \frac{u^*_{ABL}}{\sqrt{C_\mu}} \quad (6)$$

$$\varepsilon(z) = \frac{u^*_{ABL}}{\kappa(z+z_0)} \quad (7)$$

where u^*_{ABL} is the atmospheric boundary layer friction velocity, z the height above the ground, z_0 the aerodynamic roughness length, k the turbulence kinetic energy, ε the turbulence dissipation rate and $C_\mu = 0.09$ a constant of the turbulence model. A constant pressure condition is applied at the outlet boundary. At the side and top boundary, the free-slip adiabatic wall boundary condition is applied. At the bottom boundary, the no-slip adiabatic wall boundary condition is applied.

This study applied RANS $SST\ k-\omega$ model as turbulence model, which combines the advantages of standard k-ω model in the near wall region and $k-\varepsilon$ model in the far field (Menter, 1994). $SST\ k-\omega$ model has been validated and employed in our previous studies related to urban flows, air pollutant and heat dispersions (Adelia et al., 2019; Yuan and Ng, 2012; Yuan et al., 2014). Specifically, we have validated the performance of $SST\ k-\omega$ to model the anthropogenic heat dispersion by cross-comparing with wind tunnel data provided by (Allegrini et al., 2013). The validation result indicates a good agreement between the simulation result and wind tunnel data, as shown in Figure 3 (Adelia et al., 2019).

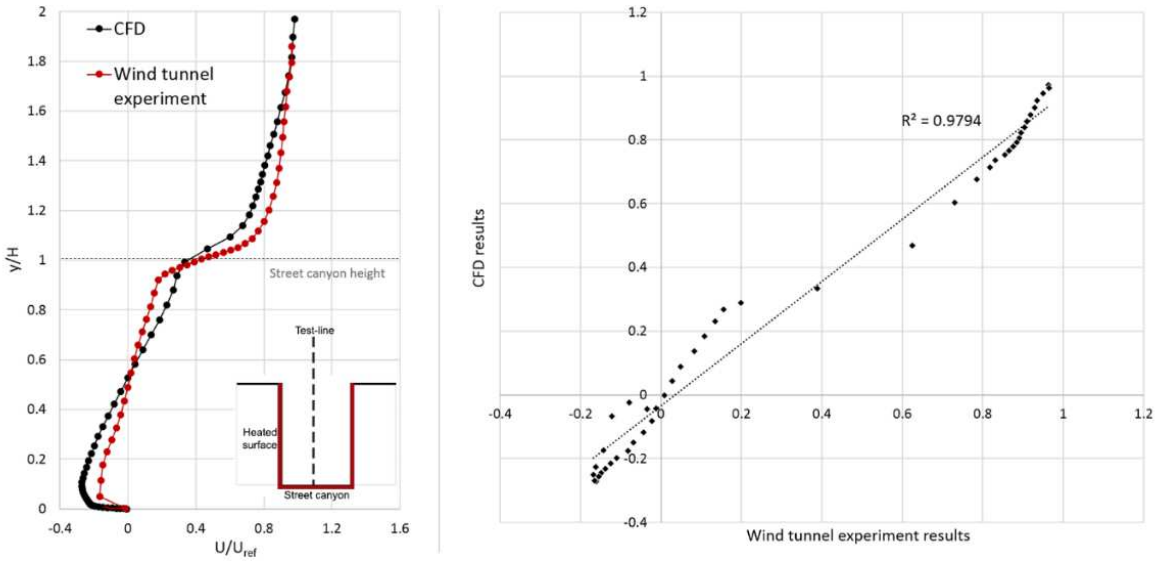

Figure 3. Validation of CFD simulations by cross-comparing with wind tunnel data. Left: modelling settings in the validation study; Right: cross-comparison result on air temperature increment.

3.4 Modelling results

Simulation results are partially presented in Figure 4, in which wind vector is overlapped on top of the air temperature contour at both vertical and horizontal planes at Case 1. Modelling results indicate that buoyancy can significantly change the flow structure inside the street canyon. As shown in Figure 4, hot air rises and exits through the street canopy opening due to buoyancy, and thus cold air horizontally enters from the sides towards the centre of the street canyon at the ground level, which is consistent with the study by Allegrini (2018). It indicates that the anthropogenic heat dispersion at the pedestrian level in the urban canopy layer could depend on site coverage ratio (λ_p), since both rooftop opening size and side entrance size of the street canyons are closely associated with λ_p.

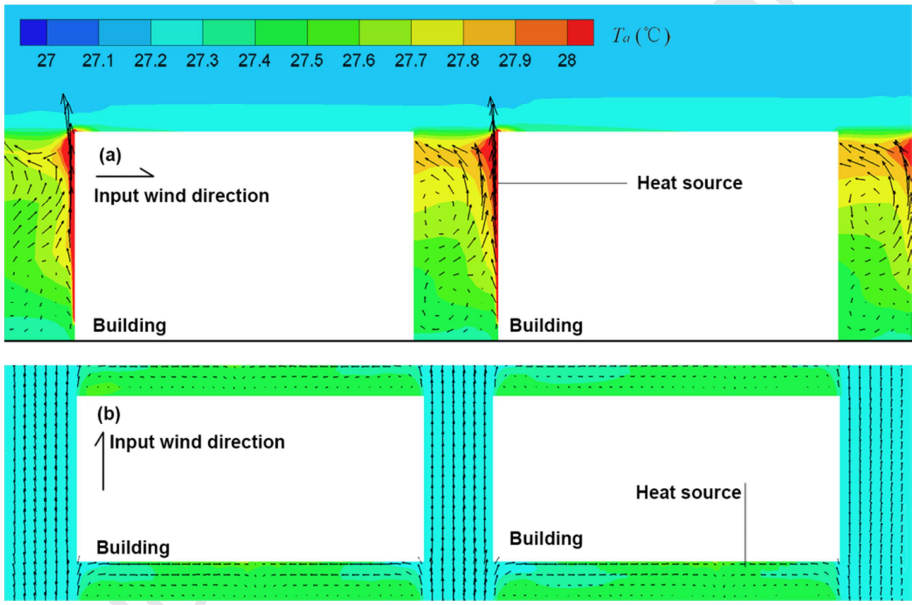

Figure 4. Air temperature contour and wind vector for Case 1 at scenario I: (a) vertical plane and (b) horizontal plane (2m above the ground).

4. Analytical Model Development

4.1 Modelling pedestrian level air temperature increment

Based on the CFD simulation results, a quantitative analysis was conducted. The increment of spatially-averaged air temperature at the pedestrian level (ΔT_p) were calculated by collecting air temperature data from horizontal test lines from both emission scenarios I and II. As shown in Figure 5, three horizontal test lines are located in the middle of street canyon. With R^2 value of 0.9, the result of linear regression analysis indicates that λ_p significantly affects ΔT_p, which decreases as λ_p decreases.

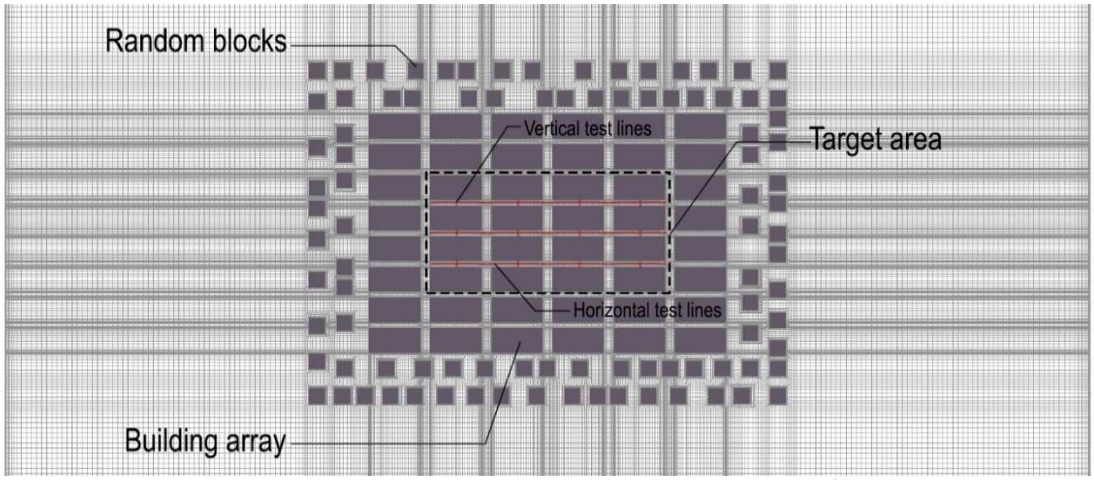

Figure 5. Location of both horizontal and vertical test lines for data and analysis. Horizontal measurement is at 2m above the ground.

We conducted simulations with input wind directions normal and parallel to the street canyons. As shown in Figure 6, as λ_p decreases, ΔT_p decreased more rapidly with the input wind direction parallel to street canyons than normal to street canyons. It is reasonable since the anthropogenic heat can be dispersed much more easily with the incoming wind parallel to streets. Specifically, the significant air temperature drop stops at λ_p 0.39, and it is almost flat afterwards. It means that, if λ_p is less than 0.39, the increment of air temperature is almost zero, with the parallel incoming wind and average heat emission at Singapore residential areas. It suggests that the optimal street orientation should be parallel with the prevailing wind direction to remove the anthropogenic heat from the street canyon. However it also should be noted that the heat could horizontally enter the leeward neighbourhood after being pushed down from the windward street canyon. Therefore, the vertical interaction between urban areas and overlying atmosphere, discussed in Section 4.2, could be more important to mitigate the negative effect of anthropogenic heat on thermal environment, especially in megacities.

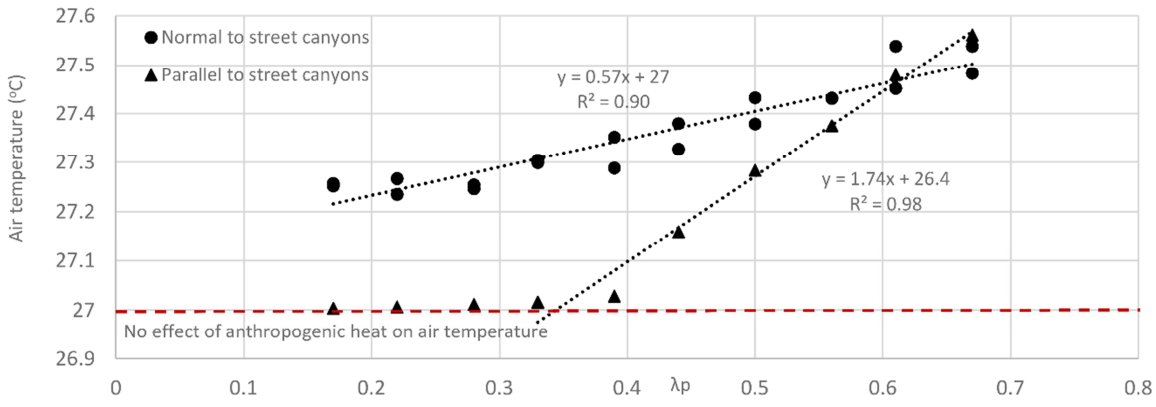

Figure 6. Regression analysis shows a strong relationship between λ_p and pedestrian level air temperature increment.

4.2 Modelling spatially-averaged in-canopy air temperature increment

Compared with the regression analysis in Section 4.1, which correlate pedestrian level ΔT_p with the average heat emission at Singapore, a new semi-empirical model is developed in this section to estimate the spatially-averaged in-canopy air temperature increment (ΔT_c) with various emission intensities. By using this new model, the effect of anthropogenic heat emission on ambient air temperature can be modelled by morphological indices, without the need to perform complicated numerical simulation. A GIS-based planning tool can be derived from this semi-empirical model to benefit urban planning practice.

The semi-empirical model was derived from a box model, based on energy conservation within the urban canopy layer. The anthropogenic heat is ejected into the canopy air volume and heats the air within it. The heat emission within the canopy layer and heat exchange between the canopy layer and the air above are shown in Figure 7. The shear stress layer at the roof level induces air exchange, which exhausts warm air and inhales cool air. There is an energy balance in the canopy layer at the steady state condition, where the anthropogenic heat emission rate Q is equal to the heat flux at roof level Q_{roof}.

$$Q = Q_{roof}, \text{where } Q_{roof} = \rho A_{opening} c_p U_E (T_c - T_0) \quad (6)$$

where, ρ is the air density, $A_{opening}$ is the opening area of urban canopy, c_p is the specific heat capacity of air, U_E is exchange velocity, T_c is the in-canopy air temperature, and T_0 is the ambient air temperature. Therefore, ΔT_c can be calculated as:

$$\Delta T_c = T_c - T_0 = \frac{Q}{\rho A_{opening} c_p U_E} \quad (7)$$

where $Q = Q_{A\_site} A_T$ and Q_{A_site} is the heat emission intensity normalized by site areas (A_T).

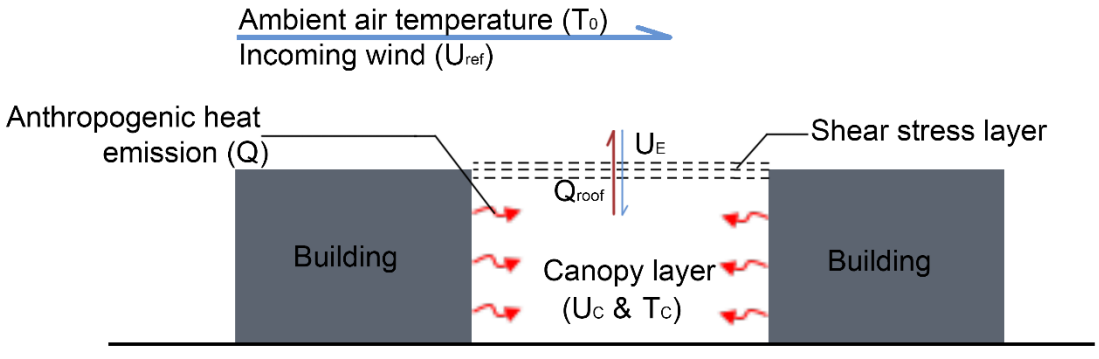

Figure 7. Schematic of the single-layer urban canopy model, derived from a box model, in which Q is equal to Q_{roof}.

The exchange velocity (U_E) needs to be solved to close equation 7. In a moderately densely packed canopy, Bentham and Britter (2003) suggested that the air exchange rate could be estimated as following:

$$\frac{U_E}{u_*} = \left(\frac{U_{ref} - U_c}{u_*}\right)^{-1} \quad (8)$$

where u_* is friction velocity, and U_c is spatially-averaged in-canopy velocity. Yuan et al. (2016) indicates that the above equation is also suitable in high density urban areas. Bentham and Britter (2003) showed that the U_c in high-density urban areas can be calculated as:

$$\frac{U_c}{u_*} = \left(\frac{2}{\lambda_f}\right)^{0.5} \quad (9)$$

The friction velocity u_* depends on the urban morphology. Yuan et al. (2016) suggested that, when λ_f is larger than 0.4, u_* is almost constant and can be evaluated as:

$$u_* = 0.12U_{ref}, where\ \lambda_f > 0.4 \quad (10)$$

Based on equations (8), (9), (10), the exchange velocity could be calculated by:

$$U_E = \frac{u_*^2}{U_{ref} - U_c} = \frac{0.0144U_{ref}}{1 - 0.12\left(\frac{2}{\lambda_f}\right)^{0.5}} \quad (11)$$

Combining Equation (7) and (11), the in-canopy air temperature increment (ΔT_c) can be calculated by urban morphology parameters λ_f and λ_p.

$$\Delta T_c = \frac{Q_{A\_site} A_T}{0.0144 U_{ref} \rho A_{opening} c_p}\left(1 - 0.12\left(\frac{2}{\lambda_f}\right)^{0.5}\right) = \frac{1}{D_c}\frac{Q_{A\_site}}{U_{ref}(1-\lambda_p)}\left(1 - 0.12\left(\frac{2}{\lambda_f}\right)^{0.5}\right) \quad (12)$$

where $D_c = 0.0144\rho c_p$ is a heat capacity constant, 17.183 ($J\,K^{-1}m^{-3}$) related to the thermal characteristics of the air.

This model was then validated by cross-comparison with the previous CFD simulation results in Section 3, as shown in the Figure 8. The in-canyon air temperature in CFD simulation were calculated by averaging the temperature collected from the vertical test lines in Figure 5. Linear regression analysis shows a good agreement between the CFD model and semi-empirical model ($R^2 = 0.69$), which indicates that this semi-empirical model can be used to estimate the increment of in-canyon air temperature caused by anthropogenic heat emission in residential areas. It should be noted that we also calculated exchange velocity

(U_E) using the Soulhac et al. (2013) model, and modelling results (ΔT_c) were included in Figure 8. It is clear that the semi-empirical model using Soulhac et al. (2013) could underestimate the ΔT_c because of overestimated U_E.

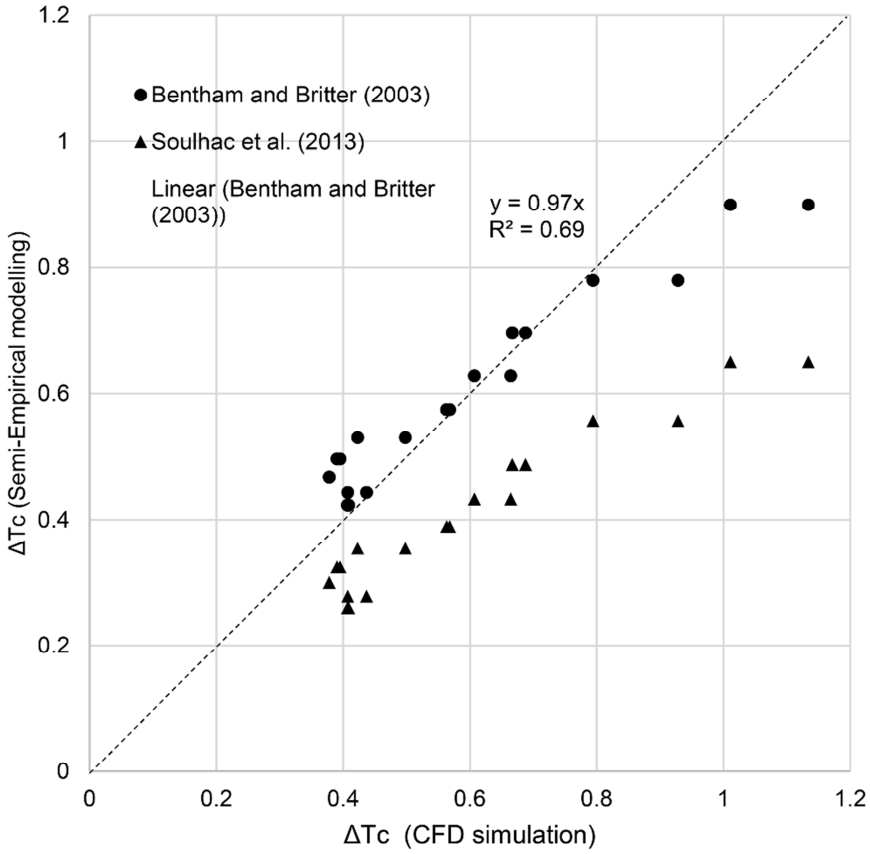

Figure 8. Cross-comparison of the in-canopy air temperature increments (ΔT_c) between the CFD and the semi-empirical model, adopting U_E estimated by both Bentham and Britter (2003) and Soulhac et al. (2013)

5. Mapping Anthropogenic Heat Impact in Residential Areas

In this section, we mapped anthropogenic heat emission and dispersion in residential areas of Singapore. As shown in Figure 9, the heat emission data, as the input data, is collected from an existing database of anthropogenic heat for Singapore (conducted by the Center for Environmental Sensing and Modelling team (CENSAM), Singapore-MIT Alliance for Research and Technology (SMART)). For HDB and condominiums, the heat emission of individual buildings was calculated based on dedicated energy consumption profiles within a postal code, which were provided by Singapore Energy Market Authority. For the landed properties, a top-down approach was adopted to calculate the heat emission from individual buildings, i.e. normalizing total energy consumption by gross floor area (GFA) as allocating factor. The 3D building geometry data, which is used to calculate GFA, is provided by AW3D company in Japan. Multiple high-resolution satellites such as DigitalGlobe WorldView

provide the satellite images that were used to utilize 3D building information. The 3D building geometry data has been successfully applied in previous research) (Dissegna et al., 2019).

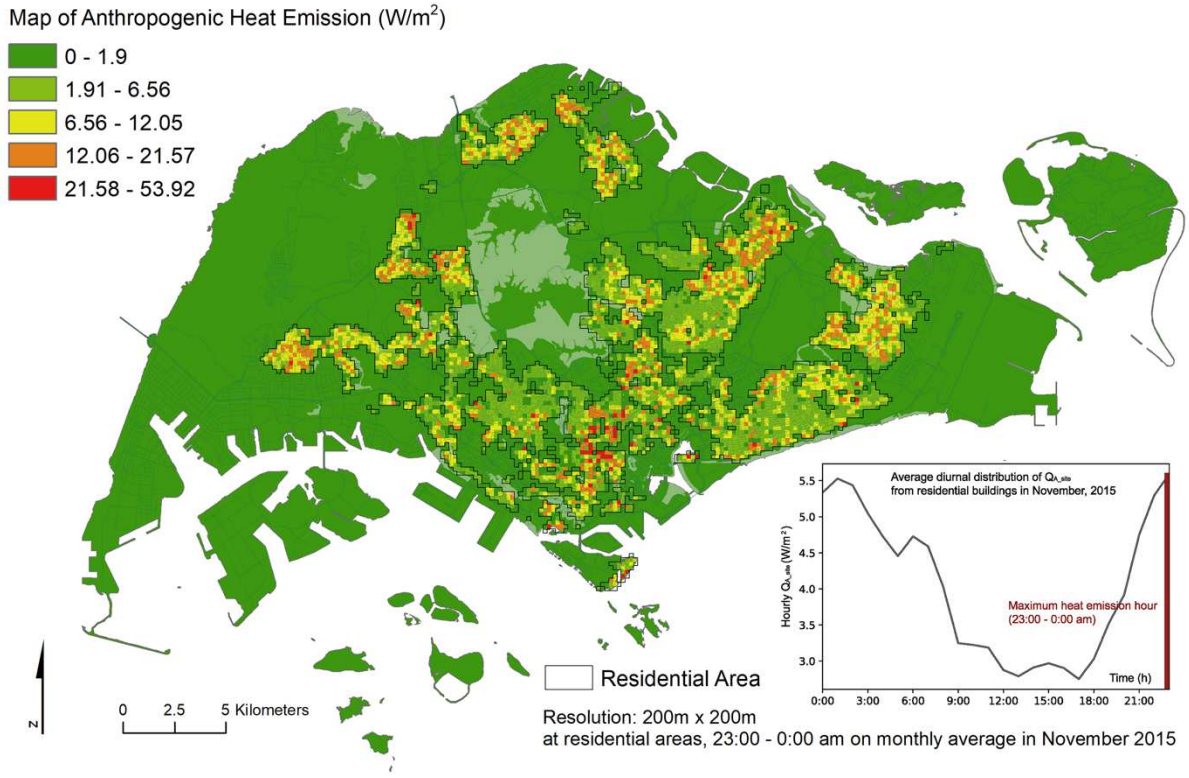

Figure 9. Map of anthropogenic heat emission from residential buildings at 23:00 – 0:00 am in November 2015. The monthly average diurnal distribution of Q_{A_site} is also presented.

Because only monthly electricity consumption data was available, the hourly electricity consumption was estimated with the help of a representative daily electricity load profile from previous study (Quah and Roth, 2012), as shown in Figure 9. For this mapping study, we chose the hour with highest emission intensity, i.e., 23:00 – 0:00 am, in the monthly average in November 2015.

Morphological indices λ_p and λ_f for residential areas of Singapore, shown in Figures 10 and 11, respectively, were calculated at each cell (200 m × 200 m), using the 3D building geometry data. In the calculation of λ_f, prevailing wind directions in November 2015 for each cell were obtained from the nearest meteorological station (Meteorological Service Singapore, 2015).

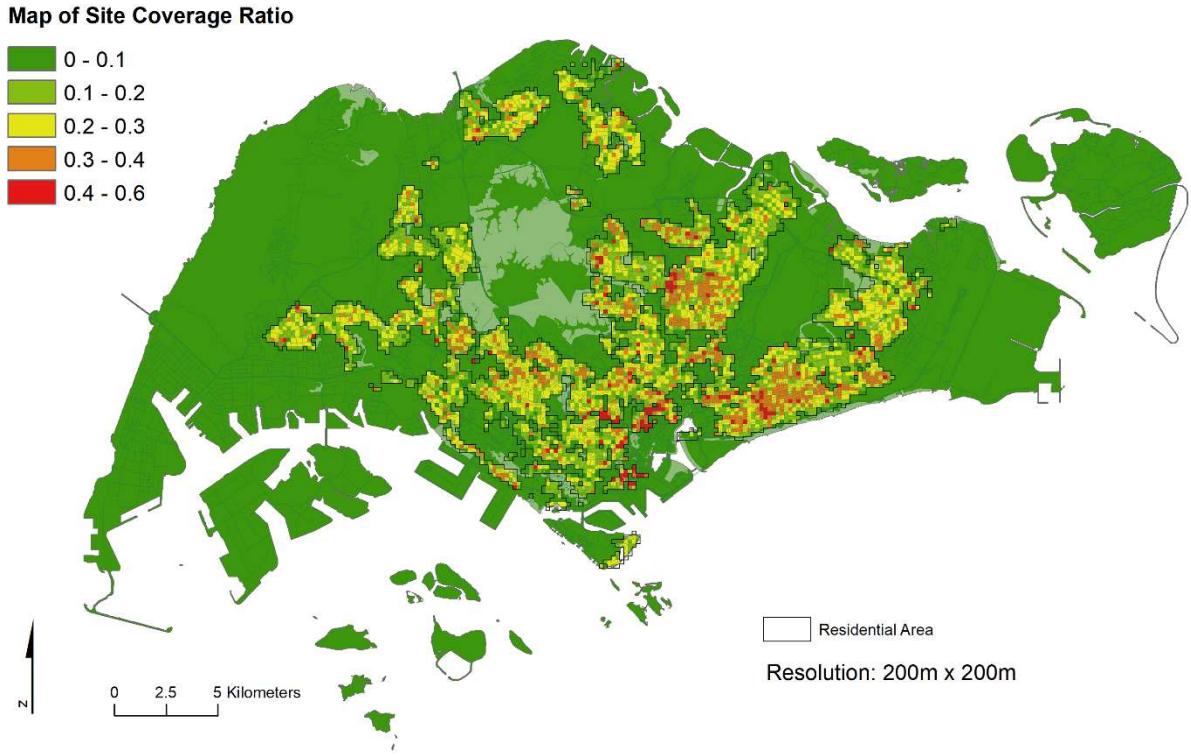

Figure 10. Map of site coverage ratio λ_p in Singapore.

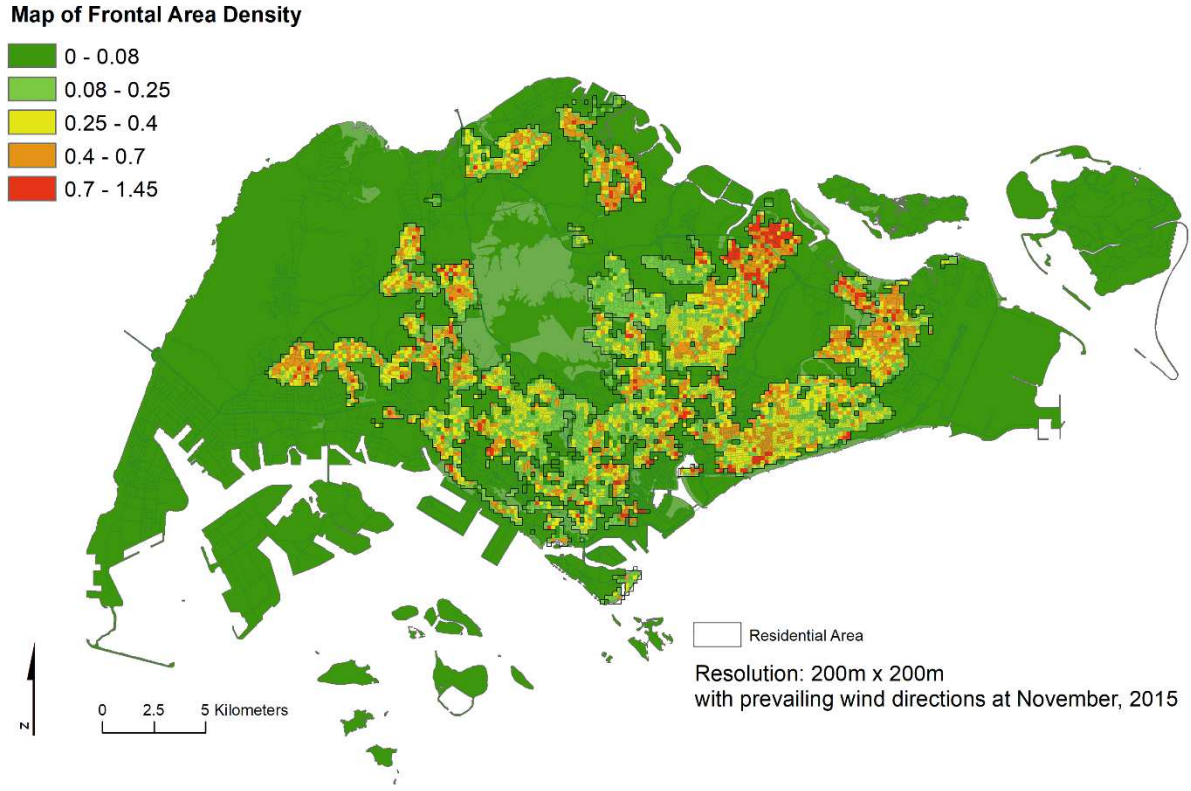

Figure 11. Map of frontal area density λ_f in Singapore. Prevailing wind directions in November 2015 from the nearest meteorological stations for each cell were applied in the λ_f calculation.

Using the new semi-empirical model developed in Section 4.2, the impact of anthropogenic heat on air temperature (ΔT_c) at residential areas was calculated in ArcGIS for scenarios with 1) annually averaged incoming wind; 2) minimum incoming wind (from 2009 to 2020). The reference wind speeds at 300m above the ground are 7.4 m/s and 1.1 m/s at scenarios I and II respectively. As shown in Figure 12a, the maximum value of ΔT_c is 0.34 °C at the downtown area, and ΔT_c is less than 0.2 °C at the most of residential areas. It indicates that anthropogenic heat has little impact on the spatially averaged air temperature in the normal, i.e. annually averaged, situation.

However, in the scenario II with high anthropogenic heat emission and very weak incoming wind, which was measured in November, 9th, 2018, the air temperature increment is much more significant than in scenario I. As shown in Figure 12b, the maximum value of ΔT_c is about 2.3°C, which is significant for outdoor thermal comfort. This grid is located near the Chinatown district, with total 1729.5kW heat emission and low dispersion potential (λ_f and λ_p are 1.02 and 0.5 respectively).

We categorized residential areas as: high, medium, and low impact zones as shown in Figure 12b. First, the areas with ΔT_c higher than 1.0°C, which is two times higher than the maximum value in the normal scenario (scenario I), are categorized as a high impact zone, about 3% of total residential areas. These areas mainly concentrated at the downtown area (Newton), Tampines, Punggol, Woodlands, Choa Chun Kang, and Jurong East. Both λ_p and Q_{A_site} at Punggol are much lower than at downtown areas, but because of higher values of λ_f, the values of ΔT_c at Punggol and downtown area are comparable. Secondly, 26 percent of residential areas with values of ΔT_c between 0.4°C to 1.0°C are categorized as a medium impact zone. Q_{A_site} at the most of these cells are higher than the mean value of residential areas, and normally λ_f is high. At last, the low impact zone with ΔT_c less than 0.4°C is occupied by low-rise buildings, such as the terrace buildings at the west region (Bukit Timah), middle area (Kovan) and the east coast region. Even though λ_p could be high at this zone, the heat emission is quite low compared with other areas.

The above analysis indicates that, if the incoming wind speed is extremely low, it is difficult for the anthropogenic heat to be dispersed. It is highly possible that heat stress risk could come from the temperature increment under an extreme situation with very low wind speed. The temperature increment in the extreme scenario (scenario II) could be 6 times higher than the scenario I.

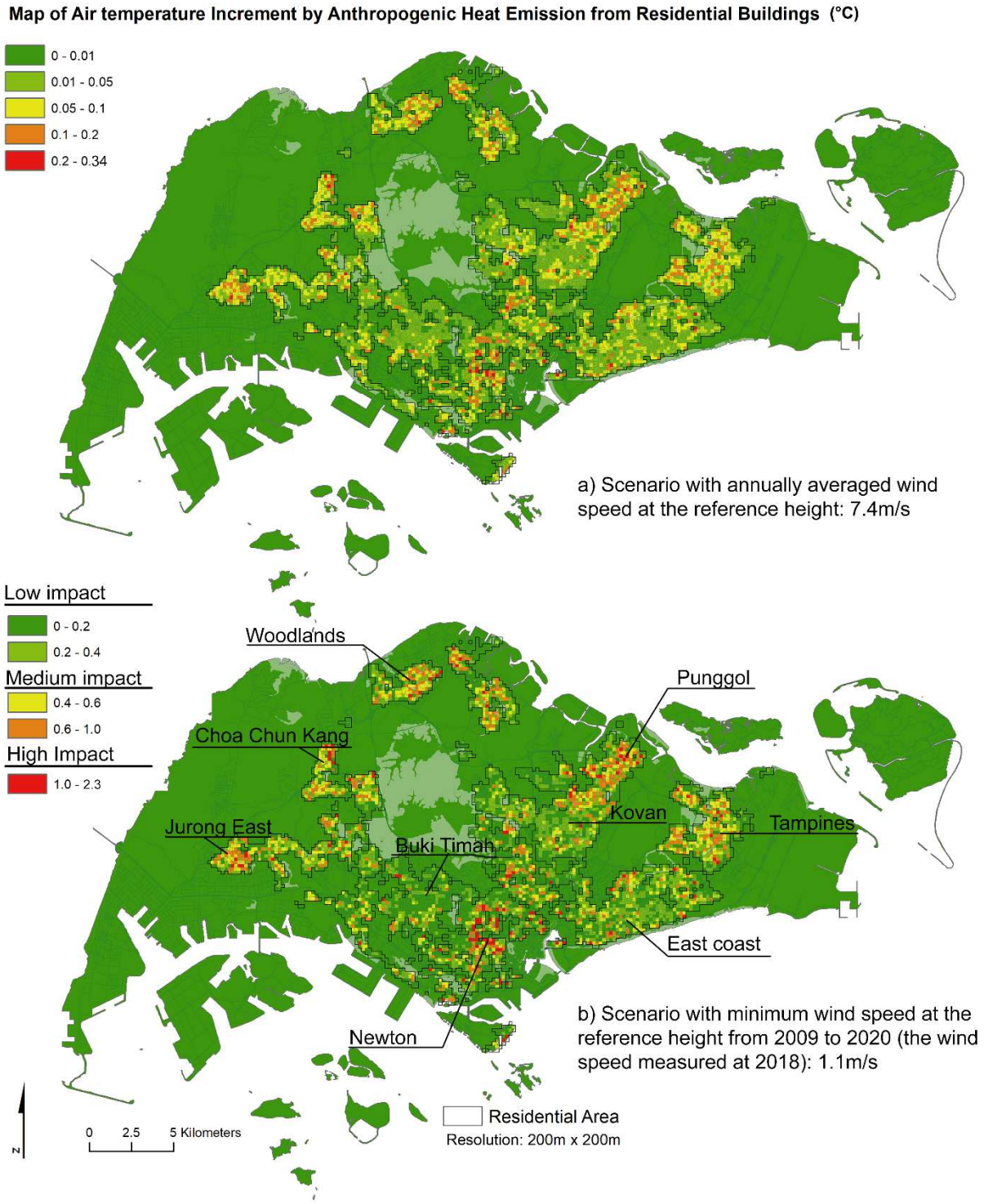

Figure 12. Map of air temperature increment (ΔT_c) at residential areas of Singapore with the heat emission at 23:00 – 0:00 on monthly average in November, 2015. Two scenarios: a) with annually averaged incoming wind; 2) with minimum incoming wind (from 2009 to 2020).

6. Conclusions

We conducted this study to support urban planning practice to mitigate the negative effect of anthropogenic heat on the microclimate in residential areas. The study is important to both urban climate sustainability and future resilience. We provided not only scientific understandings of anthropogenic heat dispersion in urban areas, but also the practical GIS-based modelling-mapping tool. This study was started by parameterizing urban morphology and conducting CFD simulations. The CFD simulation was validated by cross-comparing with the existing wind tunnel experiment results. The heat transfer and dispersion at residential areas with different morphologies, i.e. λ_p and λ_f, were simulated by the SST $SST\ k-\omega$ model in ANSYS Fluent. To associate the urban morphologies with air temperature increment, we conducted the regression analysis using CFD simulation result, and developed the GIS modelling-mapping tool. The impact of anthropogenic heat in both annually averaged and short term extreme micro climate conditions was modelled and evaluated in Singapore.

The heterogeneous urban morphologies and emission scenarios certainly bring uncertainty to the performance of new semi-empirical model. More importantly, it also should be noted that both very low wind speed and high heat emission could cause low value of Froude number, i.e. buoyance effect could dominate the heat dispersion. However, in the current model, buoyance effect is not included in the model. Consequently, ΔT_c could be overestimated in Figure 12b. More calibration and validation is still needed. Secondly, The heat storage in the building mass and urban ground surface is significant to the air temperature increment. The study on transient urban street air warming is needed. Thirdly, we will work on more parameters, such as aggregation, building and street layouts in the future study. These parameters must be helpful to improve the accuracy of the analytical model. Last but not at least, more components need to be included in the model to cover the commercial, industrial, and traffic heat emissions, which were not included in the current study but have significant impact on ambient temperature.

7. Acknowledgment

This research is supported by Singapore National Research Foundation under its two Campus for Research Excellence and Technological Enterprise (CREATE) programmes: 1) Intra-CREATE seed research grant (Grant no. NRF2018-ITS003-022) and Singapore ETH Centre, Future Resilience System II grant (Grant no. R-295-000-169-592). The computational work for this article was partially performed on resources of the National Supercomputing Centre, Singapore (https://www.nscc.sg).

8. References

Adelia, A.S., Yuan, C., Liu, L., Shan, R.Q., 2019. Effects of urban morphology on anthropogenic heat dispersion in tropical high-density residential areas. Energy and Buildings 186, 368-383.

Adolphe, L., 2001. A Simplified Model of Urban Morphology: Application to an Analysis of the Environmental Performance of Cities. Environment and Planning B: Planning and Design 28, 183-200.

Allegrini, J., 2018. A wind tunnel study on three-dimensional buoyant flows in street canyons with different roof shapes and building lengths. Building and Environment 143, 71-88.

Allegrini, J., Dorer, V., Carmeliet, J., 2013. Wind tunnel measurements of buoyant flows in street canyons. Building and Environment 59, 315-326.

Bentham, T., Britter, R., 2003. Spatially averaged flow within obstacle arrays. Atmospheric Environment 37, 2037-2043.

Chen, L., Hang, J., Sandberg, M., Claesson, L., Di Sabatino, S., Wigo, H., 2017. The impacts of building height variations and building packing densities on flow adjustment and city breathability in idealized urban models. Building and Environment 118, 344-361.

Chow, W.T.L., Roth, M., 2006. Temporal dynamics of the urban heat island of Singapore. International Journal of Climatology 26, 2243-2260.

Cui, P.-Y., Li, Z., Tao, W.-Q., 2016. Wind-tunnel measurements for thermal effects on the air flow and pollutant dispersion through different scale urban areas. Building and Environment 97, 137-151.

Dissegna, M.A., Yin, T., Wei, S., Richards, D., Grêt-Regamey, A., 2019. 3-D Reconstruction of an Urban Landscape to Assess the Influence of Vegetation in the Radiative Budget. Forests 10, 700.

Givoni, B., 1998. Climate considerations in building and urban design. John Wiley & Sons.

Grimmond, C.S.B., Oke, T.R., 1999. Aerodynamic properties of urban areas derived from analysis of surface form. Journal of applied meteorology 38, 1262-1292.

Hang, J., Luo, Z., Wang, X., He, L., Wang, B., Zhu, W., 2017. The influence of street layouts and viaduct settings on daily carbon monoxide exposure and intake fraction in idealized urban canyons. Environmental Pollution 220, 72-86.

Kikegawa, Y., Genchi, Y., Yoshikado, H., Kondo, H., 2003. Development of a numerical simulation system toward comprehensive assessments of urban warming countermeasures including their impacts upon the urban buildings' energy-demands. Applied Energy 76, 449-466.

Kim, J.-J., Baik, J.-J., 2001. Urban street-canyon flows with bottom heating. Atmospheric Environment 35, 3395-3404.

Li, X.-X., Norford, L.K., 2016. Evaluation of cool roof and vegetations in mitigating urban heat island in a tropical city, Singapore. Urban Climate 16, 59-74.

Mei, S.-J., Liu, C.-W., Liu, D., Zhao, F.-Y., Wang, H.-Q., Li, X.-H., 2016. Fluid mechanical dispersion of airborne pollutants inside urban street canyons subjecting to multi-component ventilation and unstable thermal stratifications. Science of The Total Environment 565, 1102-1115.

Menter, F.R., 1994. Two-equation eddy-viscosity turbulence models for engineering applications. AIAA journal 32, 1598-1605.

Meteorological Service Singapore, 2015. Annual Climatological Report. 1–2. .

National Environemnt Agency (NEA), 2014. Energy label and Tick Rating prior to 1 September 2014.

Ng, E., Yuan, C., Chen, L., Ren, C., Fung, J.C.H., 2011. Improving the wind environment in high-density cities by understanding urban morphology and surface roughness: A study in Hong Kong. Landscape and Urban Planning 101, 59-74.

Oke, T.R., 1988. Street design and urban canopy layer climate. Energy and Buildings 11, 103-113.

Oke, T.R., Mills, G., Christen, A., Voogt, J.A., 2017. Urban climates. Cambridge University Press.

Oliveira Panão, M.J.N., Gonçalves, H.J.P., Ferrão, P.M.C., 2009. Numerical analysis of the street canyon thermal conductance to improve urban design and climate. Building and Environment 44, 177-187.

Quah, A.K.L., Roth, M., 2012. Diurnal and weekly variation of anthropogenic heat emissions in a tropical city, Singapore. Atmospheric Environment 46, 92-103.

Richards, P.J., Hoxey, R.P., 1993. Appropriate boundary conditions for computational wind engineering models using the k-ϵ turbulence model. Journal of Wind Engineering and Industrial Aerodynamics 46-47, 145-153.

Ruck, B., 1993. Wind-tunnel measurements of flow field characteristics around a heated model building. Journal of Wind Engineering and Industrial Aerodynamics 50, 139-151.

Sini, J.-F., Anquetin, S., Mestayer, P.G., 1996. Pollutant dispersion and thermal effects in urban street canyons. Atmospheric Environment 30, 2659-2677.

Soulhac, L., Salizzoni, P., Mejean, P., Perkins, R.J., 2013. Parametric laws to model urban pollutant dispersion with a street network approach. Atmospheric Environment 67, 229-241.

Tominaga, Y., Mochida, A., Yoshie, R., Kataoka, H., Nozu, T., Yoshikawa, M., Shirasawa, T., 2008. AIJ guidelines for practical applications of CFD to pedestrian wind environment around buildings. Journal of Wind Engineering and Industrial Aerodynamics 96, 1749-1761.

Tominaga, Y., Stathopoulos, T., 2016. Ten questions concerning modeling of near-field pollutant dispersion in the built environment. Building and Environment 105, 390-402.

Tuan Seik, F., 2001. Planning and design of Tampines, an award-winning high-rise, high-density township in Singapore. Cities 18, 33-42.

Uehara, K., Murakami, S., Oikawa, S., Wakamatsu, S., 2000. Wind tunnel experiments on how thermal stratification affects flow in and above urban street canyons. Atmospheric Environment 34, 1553-1562.

Wai, K.-M., Yuan, C., Lai, A., Yu, P.K.N., 2020. Relationship between pedestrian-level outdoor thermal comfort and building morphology in a high-density city. Science of The Total Environment 708, 134516.

Yim, S.H.L., Fung, J.C.H., Lau, A.K.H., Kot, S.C., 2009. Air ventilation impacts of the “wall effect” resulting from the alignment of high-rise buildings. Atmospheric Environment 43, 4982-4994.

Yoshie, R., Tanaka, H., Shirasawa, T., Kobayashi, T., 2008. Experimental study on air ventilation in a built-up area with closely-packed high-rise buildings. Journal of Environmental Engineering (Transaction of AIJ) 73, 661-667.

Yuan, C., Ng, E., 2012. Building porosity for better urban ventilation in high-density cities – A computational parametric study. Building and Environment 50, 176-189.

Yuan, C., Ng, E., Norford, L.K., 2014. Improving air quality in high-density cities by understanding the relationship between air pollutant dispersion and urban morphologies. Building and Environment 71, 245-258.

Yuan, C., Norford, L., Britter, R., Ng, E., 2016. A modelling-mapping approach for fine-scale assessment of pedestrian-level wind in high-density cities. Building and Environment 97, 152-165.

Yuan, C., Shan, R., Zhang, Y., Li, X.-X., Yin, T., Hang, J., Norford, L., 2019. Multilayer urban canopy modelling and mapping for traffic pollutant dispersion at high density urban areas. Science of the Total Environment 647, 255-267.

Highlights

1. Urban morphology significantly affects anthropogenic heat (AH) dispersion.
2. Air temperature increment caused by AH can be estimated by site coverage ratio.
3. GIS semi-empirical model is developed to support decision making in planning.
4. Model performance is evaluated by cross-comparing with CFD simulation.
5. The effect of AH on air temperature in Singapore residential areas is mapped.

Declaration of interests

☒ The authors declare that they have no known competing financial interests or personal relationships that could have appeared to influence the work reported in this paper.

☐The authors declare the following financial interests/personal relationships which may be considered as potential competing interests: